Journal of Nuclear Materials 508 (2018) 516–520

Contents lists available at ScienceDirect

Journal of Nuclear Materials

journal homepage: www.elsevier.com/locate/jnucmat

Anisotropy in the thermal expansion of uranium silicide measured by neutron diffraction

E.G. Obbard [a, b, *], K.D. Johnson [c, 1], P.A. Burr [a, b], D.A. Lopes [c], D.J. Gregg [b], K.-D. Liss [b, 2], G. Griffiths [b], N. Scales [b], S.C. Middleburgh [d, 3]

[a] School of Electrical Engineering and Telecommunications, UNSW Sydney, NSW, 2052, Australia
[b] Australian Nuclear Science and Technology Organisation, New Illawarra Road, NSW, 2234, Australia
[c] Albanova Universitets Centrum, Kungliga Tekniska Högskolan, Stockholm, Sweden
[d] Westinghouse Electric Sweden, SE-721 63, Västerås, Sweden

HIGHLIGHTS

- In-situ neutron diffraction of U_3Si_2 during heating to 1600 °C.
- Formation of a new diffraction peak above 1000 °C not belonging to P4/mbm U_3Si_2.
- Anisotropy in expansion coincides with anomaly reported before at same temperature.
- Linear function defines reduction of thermal expansion coefficient with temperature.

GRAPHICAL ABSTRACT

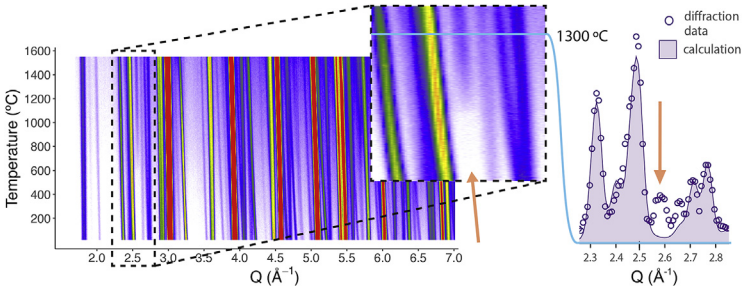

ARTICLE INFO

Article history:
Received 27 February 2018
Received in revised form
27 April 2018
Accepted 30 April 2018
Available online 30 May 2018

Keywords:
Accident tolerant fuel
In-situ neutron diffraction
Thermal expansion
Uranium silicide
Phase transformation

ABSTRACT

In-situ neutron diffraction patterns were collected for a sample of as-cast U_3Si_2 during heating to 1600 °C. Anomalous changes were observed above 1000 °C, including the formation of a new diffraction peak not belonging to *P4/mbm* U_3Si_2, unequal changes in the peak intensities and onset of anisotropic lattice expansion. The large data-set enabled derivation of a function-fitted isotropic thermal expansion coefficient to high precision, in close agreement with previous dilatometry results but reducing linearly with temperature over the studied interval. Anisotropy in the instantaneous lattice thermal expansion corresponded to anomalies reported by White et al. (2015) at a similar temperature.

Uranium Silicide (U_3Si_2) is of interest as a candidate for accident tolerant fuel [1,2], (ATF) due to its high uranium density (11.3 gm/cm^3), high thermal conductivity (~20 W/mK at 600 °C) [3], and reasonable melting point (1662 °C), when stoichiometric [4]. These advantages mean that assemblies fueled with U_3Si_2 can be designed to operate cooler (reducing fission gas release [5] and PCMI [6]) for longer residence times, at potentially lower U-235

* Corresponding author. School of Electrical Engineering and Telecommunications, UNSW Sydney, NSW, 2052, Australia.
E-mail address: e.obbard@unsw.edu.au (E.G. Obbard).
[1] Present Address: Studsvik Nuclear AB, SE-611 82 Nyköping, Sweden.
[2] Present Address: Guangdong Technion-Israel Institute of Technology, Shantou, Guangdong 515063, China; and Technion-Israel Institute of Technology, Haifa 32000, Israel.
[3] Present Address: The Nuclear Futures Institute, Bangor University, Dean Street, Bangor, Gwynedd, UK LL57 1UT.

https://doi.org/10.1016/j.jnucmat.2018.04.049
0022-3115/

enrichment levels compared to the industry standard, UO_2. There are safety benefits under normal and accident conditions, as well as overall savings in fuel cycle costs.

U_3Si_2 has been modelled using density functional theory methods [7], and is expected to be stable from room temperature to the melting point [8], without transformations in the solid state [9]. However recent thermal expansion measurements by dilatometry [3] observed a variation in the instantaneous thermal expansion coefficient between 900 °C and 1000 °C, during heating to 1500 °C. As thermal expansion is structure-sensitive this may indicate a structural transition. The thermal expansion coefficient also dictates the density of the material at a given temperature, which the calculation of thermal conductivity is dependent upon [3]. Both thermal conductivity and thermal expansion are pivotal input parameters for all fuel performance codes. Thermal expansion coefficients may be readily calculated from diffraction-measured lattice parameters under in-situ heating [10,11]. Moreover, trends in lattice strain identify phase transformations [12,13] and composition changes [14,15].

U_3Si_2 was manufactured by arc melting metallic natural uranium and pure silicon in an argon atmosphere [16,17]. Pure silicon was obtained from AlfaAesar and metallic uranium from Materials Science Corporation. Impurity analysis was performed using inductively coupled plasma optical emission spectrometry. Oxygen and nitrogen impurity levels were measured in a LECO TC436DR, and carbon in a LECO series CS440. The initial charge contained less than 100 ppm oxygen, and 400 ppm carbon. Other minor impurities such as nickel, calcium, zinc were found to be less than 25 ppm. Samples were prepared using 7.8 wt % silicon [17], a slight hyperstoichiometric content to suppress the formation of U_3Si [3] and to compensate for silicon loss during melting. The buttons were melted three times, turning between melts, followed by five additional melts to promote homogeneity within the castings.

Metallography (Olympus PMG3) in the etched condition (70/30 mixture 80% acetic acid and 65% nitric acid [18,19]), shown in Fig. 1a, revealed long, columnar grains the order of 100 μm long and 10 μm wide, typical of rapid cooling following arc melting. SEM/EDS (XL-30 Field Emission ESEM) reveals minor amounts of U-met and U_3Si phase, which appear "brighter" than the surrounding U_3Si_2 matrix in Fig. 1b. Pores and UO_2 inclusions appear black and dark grey, respectively. Image analysis of such micrographs verified a largely homogeneous melt consisting of (by volume) 99.4% U_3Si_2, 0.1% $U/U_3Si+U_3Si_2$, 0.1% UO_2 and 0.4% porosity, consistent with density and inert fusion measurements.

The sample was placed in an alumina tube with a closed end. The tube was flushed with ultra high purity (99.999%) argon three times in an enclosed, argon-filled glove bag, and sealed at the top end. The sealed tube was moved to the neutron instrument and installed in a ILL-type niobium element vacuum furnace.

Diffraction patterns were collected on the 'Wombat' high intensity powder diffractometer [20]. The sample was oscillated around the vertical axis by ± 15° to improve an otherwise 'spotty' Debye-Scherrer ring pattern caused by the cast silicide grains [21]. Temperature was ramped from ambient to 1600 °C at 5 °C per minute heating rate. Instrument parameters were refined using a NIST LaB_6 standard.

The graphical abstract shows all of the diffraction patterns from ambient to 1600 °C as a colour map [13], where diffraction intensity is scaled to colour and x and y axes are Q and temperature, respectively. Fig. 2 shows the diffraction pattern and refinement models for data collected at 1305 °C, corresponding to a slice through the colour map along a horizontal line at $y = T = 1305$ °C. Peaks from the Al_2O_3 tube, U_3Si_2 sample and the Nb heating element 110 peak are visible, as well as an unmatched peak that is observed above 900 °C (arrow on Fig. 2). This extra peak is also shown clearly by the enlargement subfigure in the graphical abstract. The Al_2O_3 phase was fit using a true Rietveld model where intensities are fixed by the structure factor calculation with an assumed random texture. For the U_3Si_2 phase, peak intensities calculated in this way did not fit the observations, likely due to significant texturing in the cast sample. U_3Si_2 peaks were therefore fit with arbitrary intensities, using the Le Bail model [22]. While most U_3Si_2 peaks form doublets with the Al_2O_3, the diffraction model for this phase is constrained between the background function and the well known Al_2O_3 peaks. Refinement constraints were progressively relaxed over four successive optimizations to refine scale parameters, lattice parameters and peak shape for crystal size and microstrain. The Al_2O_3 Debye-Waller, 'B' factors were fixed throughout and isotropic. Parameters for each pattern were refined independently. The U_3Si_2 lattice parameters at ambient temperature, obtained from a line fit to initial 50 data points are $a = 7.324$ (3) Å and $c = 3.882$ (2) Å, within 0.09% and 0.47% of previously reported U_3Si_2 lattice parameters [23]. Al_2O_3 lattice parameters a and c concur with the literature [11], within 0.08% and 0.13%.

A total of 312 pattern were obtained and refined in batch mode [24,25], to track lattice parameters and peak intensities throughout heating. The peaks progressively shift to lower Q through thermal expansion. This is shown by the off-vertical slant in the lines formed by high intensity peaks in the graphical abstract. Fig. 3 shows thermal strain $\Delta L/L_0$ for U_3Si_2 lattice parameters. The U_3Si_2 a parameter initially follows a constant expansion but the gradient of these points reduces at an intermediate temperature, signifying a change in derivative:

$$\alpha_a(T) = \frac{1}{\Delta T}\frac{\Delta a}{a_0} \quad (1)$$

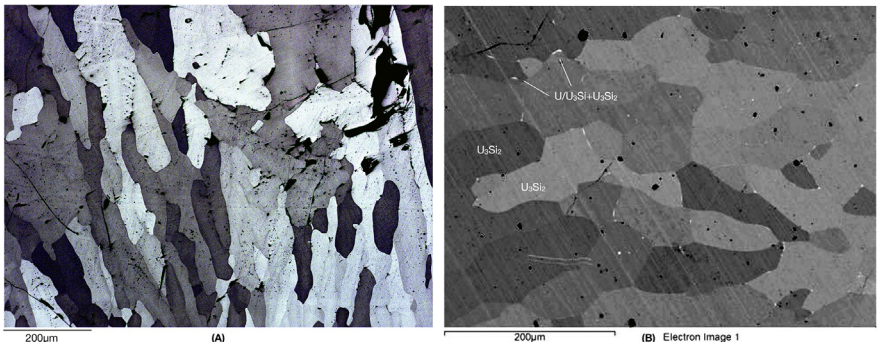

Fig. 1. (a) Optical micrograph and (b) backscattered electron SEM micrograph of as-cast U_3Si_2 sample material.

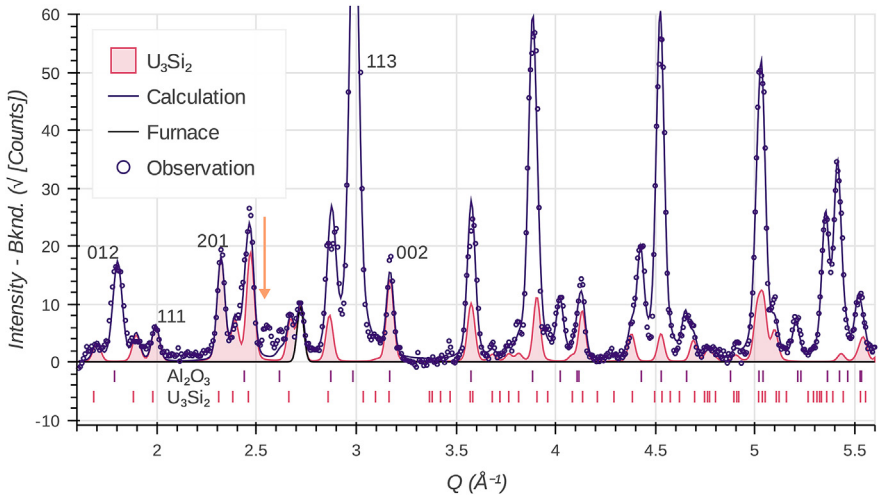

Fig. 2. Neutron diffraction pattern and Rietveld/Le Bail refinement models for U_3Si_2 in an Al_2O_3 tube at 1305 °C.

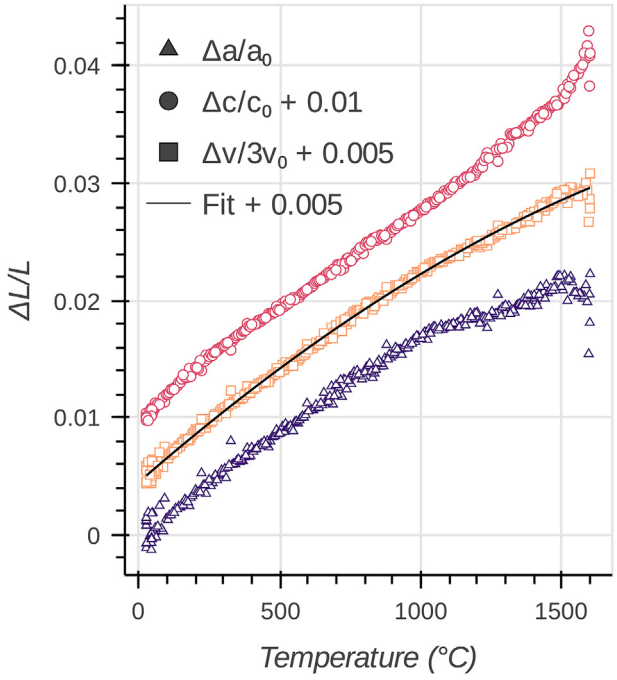

Fig. 3. Thermal strain in U_3Si_2 *a* and *c* lattice parameters and in cell volume (data for *c* and *v* are offset from *a*).

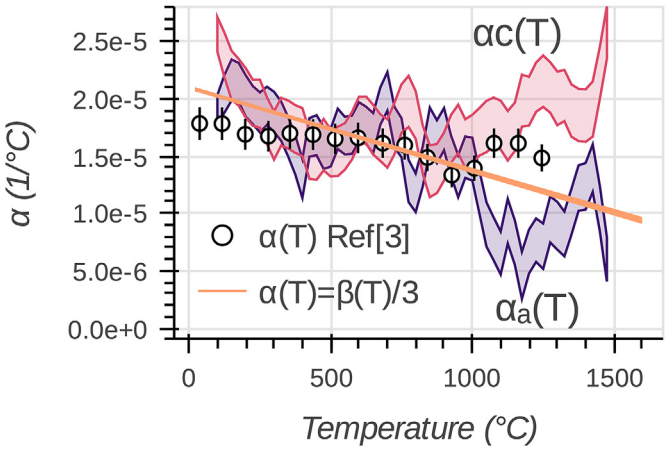

Fig. 4. Linear thermal expansion coefficients of U_3Si_2 calculated from local derivative of thermal strain and from fitting Eqn. (2) to volumetric thermal strain. Data points from [3]. Height of shading and thickness of line is their standard error. The line is $\alpha(T) = 2.10 \times 10^{-5} - 7.25 \times 10^{-9} \times T$.

This and, similarly, $\alpha_c(T)$ are calculated from linear regression of Fig. 3 strain points in a moving-window 150 °C wide. The result is the shaded regions in Fig. 4. Around 1000 °C, from an initial isotropic $\alpha \cong 1.7 \times 10^{-5}\,°C^{-1}$, $\alpha_a(T)$ reduces to ~$1.0 \times 10^{-5}\,°C^{-1}$ and $\alpha_c(T)$ increases to ~$2.0 \times 10^{-5}\,°C^{-1}$.

The true volumetric thermal expansion coefficient β and corresponding true isotropic linear thermal expansion coefficient α are defined as linear functions of temperature by:

$$\beta(T) = 3\alpha(T) = \frac{1}{V}\frac{dV}{dT} = b_0 + b_1 T \qquad (2)$$

Integration between limits V_0 and $V_0+\Delta V$ provides a fitting function that was used to find the polynomial constants for β(T). These are $b_0 = 6.2929\,(21) \times 10^{-5}$, $b_1 = -2.1760\,(15) \times 10^{-8}$ and are represented by the curve/line in Figs. 3 and 4. Fig. 4 includes the thermal expansion data points from White et al. [3].

The change in α_a coincides with the appearance of a new peak, which does not belong to the *P4/mbm* space group attributed to U_3Si_2 [26,27]. It is marked with an arrow in Fig. 2. Its intensity is tracked in Fig. 5 along with three clearly resolved U_3Si_2 peaks. Because B-factors were fixed for refinement, all peak intensities would appear to reduce smoothly with increasing temperature, and so have been normalized to the Al_2O_3 012 peak as an approximate correction for this effect. Coinciding with growth of the new peak, the U_3Si_2 002 and to a lesser extent 201 peaks begin a clear reduction in intensity around 900–1000 °C. Meanwhile 111 intensity remains constant.

Many of the U_3Si_2 diffraction peaks reduce in intensity with increasing temperature, including when compared to the Al_2O_3 peaks, which served as an internal standard to make an approximate correction for Debye-Waller factor. A simple explanation for the new peak would be formation of a new phase. An oxide produced through reaction of any available oxygen (from the gas or Al_2O_3 tube) would be one candidate. In air, U_3Si_2 oxidizes to U_3O_8 and UO_2 [28]. However the new diffraction peak does not coincide

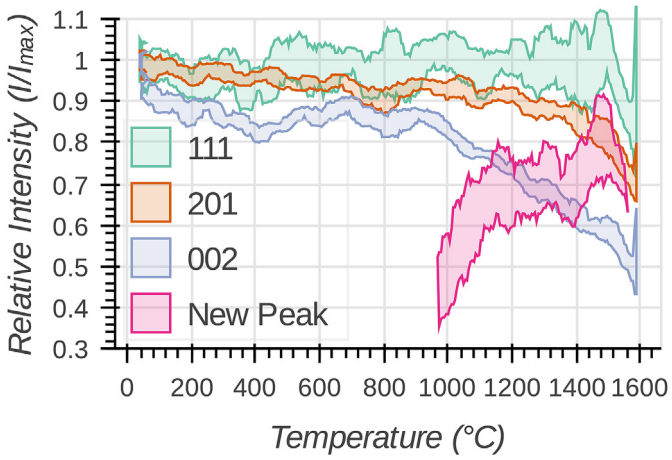

Fig. 5. Normalized intensity of selected U_3Si_2 diffraction peaks and of the unidentified peak marked by the arrow in Fig. 2; shaded area heights indicate standard error; (for b&w: series/legend order in y direction corresponds at 1000 °C).

with any peak positions of UO_2 [29], or U_3O_8 [30], including when adjusting lattice parameters for thermal expansion [10,31]. To the uranium side of U_3Si_2 intermetallic in the U-Si phase diagram [8], U_3Si, decomposes in a peritectoid reaction at 930 °C to U_3Si_2 and γ-phase uranium metal (BCC, $a = 3.48$ Å) [32]. The d-spacing of the new diffraction peak is close to the 110 peak of γ-uranium, which could indicate decomposition of $U/U_3Si+U_3Si_2$ regions to γ-$U+U_3Si_2$. The peritectoid temperature also matches the onset of changes in the diffraction patterns. The general reduction in U_3Si_2 peak intensities would support a transformation that reduced the fraction of this phase; concurrent reorientation could account for the relative changes in U_3Si_2 peak intensity. However if γ-uranium has formed, it must then melt. Yet the new peak is still observed well beyond 1135 °C, the liquidus for γ-uranium and it is doubtful that the measured, sub-0.1% fraction of Si-substoichiometic phases could account for such an observable effect. We therefore hesitate to advance a microstructural explanation for this peak.

Neutron diffraction is a bulk analysis technique because neutrons diffract from the whole sample volume. Formation of any new phase by surface oxidation or other causes does not affect the thermal expansion observations central to this experiment, which are based on lattice parameters measured from clearly identified U_3Si_2 peaks. Our fitted results for α(T) (lines, Figs. 3 and 4) match those of Ref. [3], within the reported standard error (points, Fig. 4) in the range 350–1010 °C. At lower temperatures we have measured a higher coefficient and vice versa, a trend clearly following the unit cell volume (Fig. 3). To enable comparison with early results [33–35], an average expansion coefficient [36] for a prescribed temperature range may be derived from Eqn. (2):

$$\alpha_{av} = \left[exp\left(\frac{b_0}{3}(T - T_0) + \frac{b_1}{6}\left(T^2 - T_0^2\right)\right) - 1\right] / (T - T_0) \quad (3)$$

Among these, most recent is 1.73×10^{-5} °C^{-1} [33], for 100–880 °C with cast U_3Si_2, only 1% off 1.75×10^{-5} °C^{-1} calculated by Eqn. (3).

In sintered U_3Si_2, α_{av} measured from 25 or 20 °C was observed variously to increase [34], from 1.35 to 1.50×10^{-5} °C^{-1} over the 200–1200 °C range and to decrease from 1.55 to 1.46×10^{-5} °C^{-1} over the 200–950 °C range [35]. By comparison our α_{av} for this range is higher and does not drop below minimum 1.67×10^{-5} °C^{-1} at 1200 °C. Comparing α_{av} [33–35], to α(T) can appear favorable (as in White et al. [3], who assumed fixed α over the temperature range) but is not strictly valid if α(T) is variable [36]. If calculated from a linear α(T) function based on the points of Ref. [3], in Fig. 4, ($b_0 = 5.32 \times 10^{-5}$, $b_1 = -8.04 \times 10^{-09}$), then the derived α_{av}(T) are, as for our results, also significantly higher than the older [34,35], reducing from 1.76×10^{-5} to 1.62×10^{-5} °C^{-1} over the 50–1200 °C range.

Our new measurements concur with the observation of White et al. of unexplained but significant variations in α(T) around 1000 °C. They also provide a possible explanation, which is that this temperature coincides with the onset of anisotropic thermal expansion in U_3Si_2. Agreement of unit cell volume expansion with the two most recent linear expansion results [3,33], shows that the overall isotropic thermal expansion in a polycrystal is not affected by this. However, given the observed anisotropy, significant thermal stresses must exist in the polycrystal for this to occur. The relaxation of thermal stresses by plastic deformation will affect dilatometry results and may affect the long term material performance in thermal cycling conditions. Asserting $\beta(T) = 3\alpha(T)$ for an anisotropic material is valid only for a randomly oriented polycrystal. In a textured sample overall thermal expansion would still be anisotropic, possibly explaining the observed variations including α_{av}(T) of opposite gradient [34,35].

At high temperatures, configurational entropy effects allow greater defect concentrations to be accommodated within a material. Recent modelling work identified a possible high temperature phase field above 800 °C where U_3Si_2 diverged from a line compound and may permit small changes in stoichiometry [4]. The experimentally measured aspect ratio of the unit cell in intermetallics is sensitive to variations from stoichiometry [14], and the diverging thermal expansion rates in the *a* and *c* axes observed here above 1000 °C describe a corresponding increase in the tetragonal *c/a* ratio. Entry into this newly predicted phase field on reheating, accompanied by changes in Si defect concentration is therefore one explanation for changes in thermal expansion and, if site occupancies are affected, also for changes in relative peak intensity.

A change in atomic positions would explain changes of U_3Si_2 peak intensities, thermal expansion and the new diffraction peak. The room temperature structure of U_3Si_2 was first reported as *P4/mbm* [26], and later confirmed both experimentally [27] [23], and by modelling, [7,37]. However the original work on the structure of U_3Si_2 [26], alludes to an uncertainty over the space group as either *P4/mmm* or *P4/mbm* noting that for *P4/mbm 00l* is always present but *h0l* is absent if *h* is odd. The new peak is observed close to the expected position of a *P4/mmm* 300 reflection, which at 1305 °C is at $Q = 2.52$ Å^{-1}, consistent with its position in Fig. 2.

The linear, isotropic averaged thermal expansion coefficient in U_3Si_2 measured by in-situ neutron diffraction is well described by a line $\alpha(T) = 2.10 \times 10^{-5} - 7.25 \times 10^{-9} \times T$ °C^{-1}, supporting and adding precision to two most recent measurements, but giving somewhat higher average expansion, α_{av} than older estimates. Above 1000 °C thermal expansion becomes anisotropic with reduced expansion in the *a*-axis and increased expansion in the *c*-axis, coinciding with previously observed anomalies in the thermal expansion at this temperature. This could be caused by a change in defect concentrations, or cell atomic positions and space group from *P4/mbm* to *P4/mmm*. Given the implication that anisotropy leads to thermal stresses in a polycrystal this needs to be investigated further in relation to use of U_3Si_2 as an accident tolerant fuel.

Acknowledgements

We are grateful to the Sample Environment team at the Australian Centre for Neutron Scattering, the ANSTO Nuclear Stewardship research group, and laboratory scientists and administrative staff in the Department of Reactor Physics, KTH. This work

was carried out as part of the Westinghouse CARAT collaborative project on accident tolerant fuels. PAB and EO acknowledge charitable financial support of ANSTO and the Tyree Foundation.

References

[1] S. Bragg-Sitton, Development of advanced accident-tolerant fuels for commercial LWRs, Nucl. News 57 (2014) 83.

[2] S.J. Zinkle, K.A. Terrani, J.C. Gehin, L.J. Ott, L.L. Snead, Accident tolerant fuels for LWRs: a perspective, J. Nucl. Mater. 448 (2014) 374–379.

[3] J.T. White, A.T. Nelson, J.T. Dunwoody, D.D. Byler, D.J. Safarik, K.J. Mcclellan, Thermophysical properties of U_3Si_2 to 1773 K, J. Nucl. Mater. 464 (2015) 275–280.

[4] S.C. Middleburgh, R.W. Grimes, E.J. Lahoda, C.R. Stanek, D.A. Andersson, Non-stoichiometry in U_3Si_2, J. Nucl. Mater. 482 (2016) 300–305.

[5] Y. Miao, K.A. Gamble, D. Andersson, Z.-G. Mei, A.M. Yacout, Rate theory scenarios study on fission gas behavior of U_3Si_2 under LOCA conditions in LWRs, Nucl. Eng. Des. 326 (2018) 371–382.

[6] Y. He, P. Chen, Y. Wu, G.H. Su, W. Tian, S. Qiu, Preliminary evaluation of U_3Si_2-FeCrAl fuel performance in light water reactors through a multi-physics coupled way, Nucl. Eng. Des. 328 (2018) 27–35.

[7] M.J. Noordhoek, T.M. Besmann, D. Andersson, S.C. Middleburgh, A. Chernatynskiy, Phase equilibria in the U-Si system from first-principles calculations, J. Nucl. Mater. 479 (2016) 216–223.

[8] Y.S. Kim, 3.14-Uranium intermetallic fuels (U–Al, U–Si, U–Mo), in: R.J.M. Konings (Ed.), Comprehensive Nuclear Materials, Elsevier, Oxford, 2012, pp. 391–422.

[9] A.E. Dwight, A Study of the Uranium-aluminium-silicon System, Argonne National Laboratory, 9700 South Cass Avenue, Argonne, Illinois 60439, 1982.

[10] M. Guthrie, C.J. Benmore, L.B. Skinner, O.L.G. Alderman, J.K.R. Weber, J.B. Parise, M. Williamson, Thermal expansion in UO_2 determined by high-energy X-ray diffraction, J. Nucl. Mater. 479 (2016) 19–22.

[11] G. Fiquet, P. Richet, G. Montagnac, High-temperature thermal expansion of lime, periclase, corundum and spinel, Phys. Chem. Miner. 27 (1999) 103–111.

[12] K.-D. Liss, A. Bartels, A. Schreyer, H. Clemens, High-energy X-rays: a tool for advanced bulk investigations in materials science and physics, Textures Microstruct. 35 (2003) 219–252.

[13] K. Yan, D.G. Carr, S. Kabra, M. Reid, A. Studer, R.P. Harrison, R. Dippenaar, K.-D. Liss, In situ characterization of lattice structure evolution during phase transformation of Zr-2.5Nb, Adv. Eng. Mater. 13 (2011) 882–886.

[14] L.A. Yeoh, K.-D. Liss, A. Bartels, H. Chladil, M. Avdeev, H. Clemens, R. Gerling, T. Buslaps, In situ high-energy X-ray diffraction study and quantitative phase analysis in the $\alpha+\gamma$ phase field of titanium aluminides, Scripta Mater. 57 (2007) 1145–1148.

[15] K.D. Liss, R.E. Whitfield, W. Xu, T. Buslaps, L.A. Yeoh, X. Wu, D. Zhang, K. Xia, In situ synchrotron high-energy X-ray diffraction analysis on phase transformations in Ti-Al alloys processed by equal-channel angular pressing, J. Synchrotron Radiat. 16 (2009) 825–834.

[16] K.D. Johnson, A.M. Raftery, D.A. Lopes, J. Wallenius, Fabrication and microstructural analysis of UN-U_3Si_2 composites for accident tolerant fuel applications, J. Nucl. Mater. 477 (2016) 18–23.

[17] A.-M. Raftery, Fabrication and Characterization of UN-usix Nuclear Fuel, KTH Royal Institute of Technology, 2015. https://kth.app.box.com/s/gn28kh2zkdumd8ca68r3nzhphqx9lub7.

[18] K.H. Eckelmeyer, Uranium and uranium alloys, in: G.F. Vander Voort (Ed.), ASM Handbook, vol. 9, ASM International, 9639 Kinsman Road Materials Park, Ohio, 1985, pp. 476–485. Metallography and Microstructure.

[19] G.F. Vander-Voort, Metallography, Principles and Practice, ASM International, 9639 Kinsman Road, Materials Park, Ohio, 1999.

[20] A.J. Studer, M.E. Hagen, T.J. Noakes, Wombat: the high-intensity powder diffractometer at the OPAL reactor, Phys. B Condens. Matter 385–386 (2006) 1013–1015.

[21] K.-D. Liss, K. Yan, Thermo-mechanical processing in a synchrotron beam, Mater. Sci. Eng. 528 (2010) 11–27.

[22] A. Le Bail, Whole powder pattern decomposition methods and applications: a retrospection, Powder Diffr. 20 (2005) 316–326.

[23] R.C. Birtcher, J.W. Richardson, M.H. Mueller, Amorphization of U_3Si_2 by ion or neutron irradiation, J. Nucl. Mater. 230 (1996) 158–163.

[24] L. Lutterotti, S. Matthies, H.R. Wenk, MAUD (material analysis using diffraction): a user friendly Java program for Rietveld texture analysis and more, in: Proceeding of the Twelfth International Conference on Textures of Materials (ICOTOM-12), NRC Research Press, Ottowa, Canada, 1999, p. 1599.

[25] L. Lutterotti, Quantitative Rietveld analysis in batch mode with Maud, and new features in Maud 2.037, IUCR CPD Newsletter 32 (2005) 53–55.

[26] W.H. Zachariasen, Crystal chemical studies of the 5f-series of elements. VIII. Crystal structure studies of uranium silicides and of $CeSi_2$, $NpSi_2$, and $PuSi_2$, Acta Crystallogr. 2 (1949) 94–99.

[27] K. Remschnig, T. Le Bihan, H. Noël, P. Rogl, Structural chemistry and magnetic behavior of binary uranium silicides, J. Solid State Chem. 97 (1992) 391–399.

[28] E. Sooby Wood, J.T. White, A.T. Nelson, Oxidation behavior of U-Si compounds in air from 25 to 1000 C, J. Nucl. Mater. 484 (2017) 245–257.

[29] G. Leinders, T. Cardinaels, K. Binnemans, M. Verwerft, Accurate lattice parameter measurements of stoichiometric uranium dioxide, J. Nucl. Mater. 459 (2015) 135–142.

[30] J.B. Ainscough, I.F. Ferguson, The oxidation of uranium dioxide-yttria solid solutions, J. Inorg. Nucl. Chem. 36 (1974) 193–194.

[31] R.J. Ackermann, A.T. Chang, C.A. Sorrell, Thermal expansion and phase transformations of the U_3O_8–z phase in air, J. Inorg. Nucl. Chem. 39 (1977) 75–85.

[32] A.S. Wilson, R.E. Rundle, The structures of uranium metal, Acta Crystallogr. 2 (1949) 126–127.

[33] H. Shimizu, The Properties and Irradiation Behavior of U_3Si_2, in: NAA-sr-10621, Atomics International, Canoga Park, Calif., United States, 1965, https://doi.org/10.2172/4639974.

[34] K.M. Taylor, C.H. McMurtry, Synthesis and fabrication of refractory uranium compounds, in: Summary Report for May 1959 through December 1960, Carborundum Company, Niagara Falls, New York, United States, 1961.

[35] L.D. Loch, G.B. Engle, M.J. Snyder, W.H. Duckworth, Survey of Refractory Uranium Compounds, Report BMI-1124, Batelle Memorial Institute, 505 King Avenue Columbus 1, Ohio, 1956.

[36] J.D. James, J.A. Spittle, S.G.R. Brown, R.W. Evans, A review of measurement techniques for the thermal expansion coefficient of metals and alloys at elevated temperatures, Meas. Sci. Technol. 12 (2001). R1.

[37] T. Wang, N. Qiu, X. Wen, Y. Tian, J. He, K. Luo, X. Zha, Y. Zhou, Q. Huang, J. Lang, S. Du, First-principles investigations on the electronic structures of U_3Si_2, J. Nucl. Mater. 469 (2016) 194–199.